

# Anomalous Andreev bound state in non-centrosymmetric superconductors

Yukio Tanaka<sup>1</sup>, Yoshihiro Mizuno<sup>1</sup>, Takehito Yokoyama<sup>2</sup>, Keiji Yada<sup>1</sup>, and Masatoshi Sato<sup>3</sup>

<sup>1</sup>Department of Applied Physics, Nagoya University, Nagoya, 464-8603, Japan

<sup>2</sup>Department of Physics, Tokyo Institute of Technology, Tokyo, 152-8551, Japan

<sup>3</sup>Institute for Solid State Physics, University of Tokyo, Chiba 277-8581, Japan

(Dated: July 20, 2010)

We study edge states of non-centrosymmetric superconductors where spin-singlet  $d$ -wave pairing mixes with spin-triplet  $p$  (or  $f$ )-wave one by spin-orbit coupling. For  $d_{xy}$ -wave pairing, the obtained Andreev bound state has an anomalous dispersion as compared to conventional helical edge modes. A unique topologically protected time-reversal invariant Majorana bound state appears at the edge. The charge conductance in the non-centrosymmetric superconductor junctions reflects the anomalous structures of the dispersions, particularly the time-reversal invariant Majorana bound state is manifested as a zero bias conductance peak.

PACS numbers: 74.45.+c, 74.50.+r, 74.20.Rp

Recently, physics of non-centrosymmetric (NCS) superconductors is one of the important issues in condensed matter physics [1–4]. One of the remarkable features in NCS superconductors is that due to the broken inversion symmetry, superconducting pair potential becomes a mixture of spin-singlet even-parity and spin-triplet odd-parity [5]. Due to the mixture of spin-singlet and spin-triplet pairings, several novel properties such as the large upper critical field are expected [3, 6].

Up to now, there have been several studies about superconducting profiles of NCS superconductors [3, 6–13]. In these works, pairing symmetry of NCS superconductors has been mainly assumed to be  $s + p$ -wave. However, in a strongly correlated system, this assumption is not valid anymore. Microscopic calculations have shown that  $d_{x^2-y^2}$ -wave spin-singlet pairing mixes with  $f$ -wave pairing based on the Hubbard model near half filling [14]. Also, a possible pairing symmetry of superconductivity generated at heterointerface  $\text{LaAlO}_3/\text{SrTiO}_3$  [4] has been studied based on a similar model [15]. It has been found that the gap function consists of spin-singlet  $d_{xy}$ -wave component and spin-triplet  $p$ -wave one [15]. Therefore, now, it is a challenging issue to reveal novel properties specific to  $d_{xy} + p$  or  $d_{x^2-y^2} + f$ -wave pairing.

The generation of Andreev bound state (ABS) at the surface or interface is a significantly important feature specific to unconventional pairing since ABS directly manifests itself in the tunneling spectroscopy. Actually, for  $d_{xy}$ -wave pairing, zero energy dispersionless ABS appears [16]. The presence of ABS has been verified by tunneling experiments of high- $T_c$  cuprate [17] as a zero bias conductance peak (ZBCP). For NCS superconductors, when  $p$ -wave pair potential is larger than  $s$ -wave one, it has been shown that ABS is generated at its edge as helical edge modes similar to those in quantum spin Hall system [9–12]. Several new features of spin transport stemming from these helical edge modes have been also predicted [10–13]. However, there has been no theory about ABS in  $d_{xy} + p$ - or  $d_{x^2-y^2} + f$ -wave pairing in

NCS superconductors. Since tunneling spectroscopy via ABS [16] is a powerful method to identify pairing symmetry and mechanism of unconventional superconductors [17], it is quite important and interesting to clarify ABS and resulting tunneling conductance for  $d_{xy} + p$ -wave and  $d_{x^2-y^2} + f$ -wave pairings.

In this Letter, we investigate ABS and tunneling conductance  $\sigma_C$  in normal metal / NCS superconductor junctions. For both  $d_{xy} + p$ -wave and  $d_{x^2-y^2} + f$ -wave cases, new types of ABS are obtained. In particular, for  $d_{xy} + p$ -wave case, due to the Fermi surface splitting by spin-orbit coupling, a single branch of topologically stable Majorana bound state appears. Recently, to search for Majorana fermions is one of the hottest issues in condensed matter physics [18, 19]. In stark contrast to the other Majorana fermions, the present one preserves time-reversal symmetry. From this difference, the “time-reversal invariant (TRI) Majorana bound state” has a peculiar flat dispersion. It shows a unique ZBCP in  $\sigma_C$  depending on the spin-orbit coupling. Therefore, the experimental identification is feasible.

We start with the Hamiltonian of NCS superconductor

$$\hat{H}_S = \begin{pmatrix} \hat{H}(\mathbf{k}) & \hat{\Delta}(\mathbf{k}) \\ -\hat{\Delta}^*(-\mathbf{k}) & -\hat{H}^*(-\mathbf{k}) \end{pmatrix} \quad (1)$$

with  $\hat{H}(\mathbf{k}) = \xi_{\mathbf{k}} + \mathbf{V}(\mathbf{k}) \cdot \hat{\boldsymbol{\sigma}}$ ,  $\mathbf{V}(\mathbf{k}) = \lambda(\hat{x}k_y - \hat{y}k_x)$ ,  $\xi_{\mathbf{k}} = \hbar^2 \mathbf{k}^2 / (2m) - \mu$ . Here,  $\mu$ ,  $m$ ,  $\hat{\boldsymbol{\sigma}}$  and  $\lambda$  denote chemical potential, effective mass, Pauli matrices and coupling constant of Rashba spin-orbit interaction, respectively [3]. The pair potential  $\hat{\Delta}(\mathbf{k})$  is given by  $\hat{\Delta}(\mathbf{k}) = [\mathbf{d}(\mathbf{k}) \cdot \hat{\boldsymbol{\sigma}}]i\hat{\sigma}_y + i\psi(\mathbf{k})\hat{\sigma}_y$ . Due to the spin-orbit coupling, the spin-triplet component  $\mathbf{d}(\mathbf{k})$  is aligned with the polarization vector of the Rashba spin orbit coupling,  $\mathbf{d}(\mathbf{k}) \parallel \mathbf{V}(\mathbf{k})$  [3]. Then, the triplet component is  $\mathbf{d}(\mathbf{k}) = \Delta_t f(\mathbf{k})(\hat{x}k_y - \hat{y}k_x)/k$  with  $k = \sqrt{\mathbf{k}^2}$  while singlet component reads  $\psi(\mathbf{k}) = \Delta_s f(\mathbf{k})$  with  $\Delta_t \geq 0$  and  $\Delta_s \geq 0$ .  $f(\mathbf{k})$  is given by  $f(\mathbf{k}) = 2k_x k_y / k^2$  for  $d_{xy} + p$ -wave and  $f(\mathbf{k}) = (k_x^2 - k_y^2) / k^2$  for  $d_{x^2-y^2} + f$ -wave. [20] The superconducting gaps are  $\Delta_1 = |\bar{\Delta}_1(\mathbf{k})|$  and  $\Delta_2 = |\bar{\Delta}_2(\mathbf{k})|$  for

the two spin-split band with  $\bar{\Delta}_1(\mathbf{k}) = (\Delta_t + \Delta_s)f(\mathbf{k})$  and  $\bar{\Delta}_2(\mathbf{k}) = (\Delta_t - \Delta_s)f(\mathbf{k})$ , respectively, in homogeneous state [9].

Let us consider a wave function including ABS localized at the surface. Consider a two-dimensional semi-infinite superconductor on  $x > 0$  where the surface is located at  $x = 0$ . The corresponding wave function is given by [11]

$$\begin{aligned} \Psi_S(x) &= [c_1^+ \psi_1^+ \exp(iq_{1x}^+ x) + c_1^- \psi_1^- \exp(-iq_{1x}^- x) \\ &+ c_2^+ \psi_2^+ \exp(iq_{2x}^+ x) + c_2^- \psi_2^- \exp(-iq_{2x}^- x)] \exp(ik_y y), \quad (2) \\ q_{1(2)x}^\pm &= k_{1(2)x}^\pm \pm \frac{k_{1(2)}^\pm}{k_{1(2)x}^\pm} \sqrt{\frac{E^2 - [\bar{\Delta}_{1(2)}(\mathbf{k}_{1(2)}^\pm)]^2}{\lambda^2 + 2\hbar^2 \mu/m}}, \end{aligned}$$

with  $k_{1(2)x}^+ = k_{1(2)x}^- = \sqrt{k_{1(2)}^2 - k_y^2}$  for  $|k_y| \leq k_{1(2)}$  and  $k_{1(2)x}^+ = -k_{1(2)x}^- = i\sqrt{k_y^2 - k_{1(2)}^2}$  for  $|k_y| > k_{1(2)}$ , and  $\mathbf{k}_{1(2)}^\pm = (\pm k_{1(2)x}^\pm, k_y)$ . Here,  $k_1$  and  $k_2$  are the Fermi wavenumbers for the smaller and larger Fermi surface given by  $-m\lambda/\hbar^2 + \sqrt{(m\lambda/\hbar^2)^2 + 2m\mu/\hbar^2}$  and  $m\lambda/\hbar^2 + \sqrt{(m\lambda/\hbar^2)^2 + 2m\mu/\hbar^2}$ , respectively. The wave functions are given by  ${}^T\psi_1^\pm = (1, -i\alpha_{1\pm}^{-1}, i\alpha_{1\pm}^{-1}\Gamma_{1\pm}, \Gamma_{1\pm})$  and  ${}^T\psi_2^\pm = (1, i\alpha_{2\pm}^{-1}, i\alpha_{2\pm}^{-1}\Gamma_{2\pm}, -\Gamma_{2\pm})$  with

$$\Gamma_{1(2)\pm} = \frac{\bar{\Delta}_{1(2)}(\mathbf{k}_{1(2)}^\pm)}{E \pm \sqrt{E^2 - [\bar{\Delta}_{1(2)}(\mathbf{k}_{1(2)}^\pm)]^2}}, \quad (3)$$

and  $\alpha_{1(2)\pm} = (\pm k_{1(2)x}^\pm - ik_y)/k_{1(2)}$ .  $E$  is the quasiparticle energy measured from the Fermi energy.

Postulating  $\Psi_S(x) = 0$  at  $x = 0$ , we can determine the ABS. We consider the case for  $|k_y| < k_2$ . We first focus on the ABS for  $d_{xy} + p$ -wave case. For  $\Delta_t > \Delta_s$ , the dispersion  $\varepsilon_b$  of ABS is given by

$$\varepsilon_b = \begin{cases} \frac{\pm 2\Delta_t \gamma \sqrt{(k_1^2 - k_y^2)(k_2^2 - k_y^2)(k_y^2 - \eta^2 k_1^2)}}{(k_1 + k_2)k_1 k_2} & k_c < |k_y| \leq k_1 \\ 0 & k_1 < |k_y| \end{cases} \quad (4)$$

with  $\gamma = (k_1/k_2 + k_2/k_1) + (\Delta_s/\Delta_t)(k_2/k_1 - k_1/k_2)$ ,  $\eta = [\Delta_t(1 - k_1/k_2) + \Delta_s(1 + k_1/k_2)]/\{\Delta_t[1 + (k_1/k_2)^2] + \Delta_s[1 - (k_1/k_2)^2]\}$ ,  $k_c = k_1\sqrt{\Delta_t(1 - k_1/k_2) + \Delta_s}/\sqrt{\Delta_t + \Delta_s[1 - (k_1/k_2)^2]}$ . On the other hand, for  $\Delta_s > \Delta_t$ , the resulting  $\varepsilon_b$  is given by  $\varepsilon_b = 0$ . The dispersion  $\varepsilon_b$  of ABS changes drastically at  $\Delta_s = \Delta_t$ , where one of the energy gaps, i.e.  $\Delta_2$ , becomes zero. It should be remarked that the present ABSs do not break the time reversal symmetry.

The resulting  $\varepsilon_b$  is plotted for various cases in Fig. 1 with  $\Delta_0 = \Delta_s + \Delta_t$ . For convenience, we introduce dimensionless constant  $\beta = 2m\lambda/(\hbar^2 k_f)$  with  $k_f = \sqrt{2m\mu/\hbar^2}$ . We also plot  $\Delta_1$  and  $\Delta_2$ . Both  $\Delta_1$  and  $\Delta_2$  become zero at  $k_y = 0$ . At  $|k_y| = k_2$ ,  $\Delta_2$  is always zero. However,  $\Delta_1$  then becomes zero only for  $\beta = 0$ . First,

we look at the  $\Delta_t > \Delta_s$  case. For  $\Delta_s = 0$  with  $\beta = 0$ ,  $\varepsilon_b = \pm ck_y$  with some constant  $c$  for small  $k_y$  (curve  $a$  in Fig. 1(A)) as shown in the case of  $s+p$ -wave pairing[8–13] since  $\eta = 0$  is satisfied. This type of ABS is called helical edge mode [11, 12, 21]. However, this condition is satisfied only for  $\Delta_s = 0$  and  $\beta = 0$ . In fact,  $\varepsilon_b$  near  $k_y = 0$  becomes absent in general as shown in curves  $a$  in Figs. 1(B), (D) and (E). At  $k = \pm k_c$ ,  $\varepsilon_b$  coincides with  $\pm\Delta_2$ . For nonzero  $\beta$ ,  $\varepsilon_b$  becomes exactly zero for  $|k_y| > k_1$  as shown in curves  $a$  in Figs. 1(D) and (E). The present line shapes of  $\varepsilon_b$  are completely different from those of  $s + p$ -wave superconductors. On the other hand, for  $\Delta_s > \Delta_t$ ,  $\varepsilon_b = 0$  for any  $k_y$  similar to the case of spin-singlet  $d_{xy}$  or spin-triplet  $p_x$ -wave pairing [16, 17].

We notice here that the zero energy bound state for  $|k_y| > k_1$  is a Majorana bound state. The wave function for the zero energy edge state  $\Psi_m(k_y)$  can be written as  ${}^T\Psi_m(k_y) = (u_1(k_y), u_2(k_y), v_1(k_y), v_2(k_y))$  where

$$u_1(k_y) = -i\sigma v_2(k_y) = \frac{(\alpha f_1 - \beta_1 f_2) \exp(ik_y y - i\frac{\pi}{4})}{\sqrt{\sigma\alpha}} \quad (5)$$

$$u_2(k_y) = i\sigma v_1(k_y) = \frac{(f_1 + \beta_2 f_2) \exp(ik_y y - i\frac{\pi}{4})}{\sqrt{\sigma\alpha}} \quad (6)$$

with  $\alpha = (k_y - \sqrt{k_y^2 - k_1^2})/k_1$ ,  $\beta_1 = (\alpha k_y/k_2 + 1)$ ,  $\beta_2 = (\alpha + k_y/k_2)$  and  $\sigma = \text{sgn}(k_y)$ . The functions  $f_1$  and  $f_2$  decays exponentially as a function of  $x$  and are even function of  $k_y$ . The Bogoliubov quasiparticle creation operator for this state is constructed in the usual way as  $\gamma^\dagger(k_y) = u_1(k_y)c_\uparrow^\dagger(k_y) + u_2(k_y)c_\downarrow^\dagger(k_y) + v_1(k_y)c_\uparrow(-k_y) + v_2(k_y)c_\downarrow(-k_y)$ . Since  $u_1(k_y) = v_1^*(-k_y)$  and  $u_2(k_y) = v_2^*(-k_y)$  are satisfied, it is possible to verify that  $\gamma^\dagger(k_y) = \gamma(-k_y)$ . This means the generation of Majorana bound state at the edge for  $|k_y| > k_1$ . For  $\Delta_s > \Delta_t$ , a similar Majorana bound state also appears for  $|k_y| > k_1$ . On the other hand, for  $|k_y| \leq k_1$ , Majorana bound state has double branches and it is reduced to be conventional zero energy ABS.

Unlike Majorana fermions studied before [18, 19], the present single Majorana bound state is realized with time reversal symmetry. The TRI Majorana bound state has the following three characteristics. a) It has a unique flat dispersion: To be consistent with the time-reversal invariance, the single branch of zero mode should be symmetric under  $k_y \rightarrow -k_y$ . Therefore, by taking into account the particle-hole symmetry as well, the flat dispersion is required. On the other hand, the conventional time-reversal breaking Majorana bound state has a linear dispersion. b) The spin-orbit coupling is necessary to obtain the TRI Majorana bound state. Without spin-orbit coupling, the TRI Majorana bound state vanishes. c) The TRI Majorana bound state is topologically stable under small deformations of the Hamiltonian (1).

We also calculate ABS for  $d_{x^2-y^2} + f$ -wave case. In this case, ABS exists only for  $\Delta_s < \Delta_t$ . In Fig. 2,  $\varepsilon_b$  is plotted similarly to Fig. 1. As a reference, corresponding

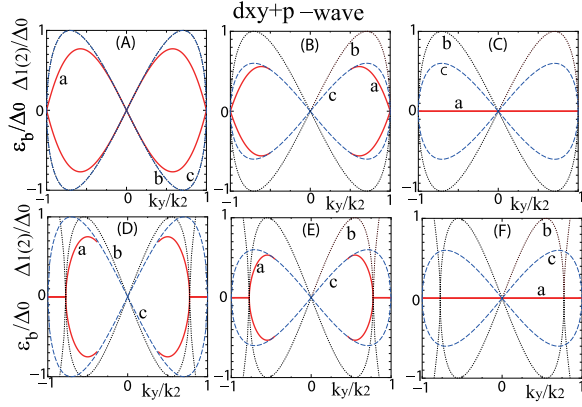


FIG. 1: (Color online) Andreev bound state  $\varepsilon_b$ , effective pair potentials for each Fermi surface  $\Delta_1$  and  $\Delta_2$  are plotted for  $d_{xy} + p$ -wave case as a function of  $k_y/k_2$ .  $\beta = 0$  for panels A, B and C.  $\beta = 0.5$  for panels D, E and F.  $\Delta_t = \Delta_0$ ,  $\Delta_s = 0$  for A and D.  $\Delta_t = 0.8\Delta_0$ ,  $\Delta_s = 0.2\Delta_0$  for B and E.  $\Delta_t = 0.2\Delta_0$ ,  $\Delta_s = 0.8\Delta_0$ , for C and F. In all panels, curves a (solid line), b (dotted line) and c (dashed line) denote  $\varepsilon_b/\Delta_0$ ,  $\Delta_1/\Delta_0$  and  $\Delta_2/\Delta_0$ , respectively.

$\varepsilon_b$  is also shown for  $s + p$ -wave case. Helical edge modes around  $k_y = 0$  exist and  $\varepsilon_b$  is absorbed into continuum levels for  $|k_y| > k_1$ . These features are similar to those of  $s + p$ -wave case. However, the number of crossing points of  $\varepsilon_b$  is five for  $d_{x^2-y^2} + f$ -wave case reflecting the complex  $\mathbf{k}$ -dependence of the pair potential. The overall line shapes of  $\varepsilon_b$  (curve a) in Fig. 2(A) is significantly different from corresponding  $\varepsilon_b$  (curve a) in Fig. 2(B).

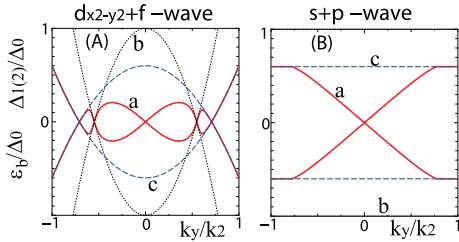


FIG. 2: (Color online) Similar plots to Fig. 1 with  $\beta = 0.5$  for  $d_{x^2-y^2} + f$ -wave (A) and  $s + p$ -wave case (B) with  $\Delta_t = 0.8\Delta_0$ ,  $\Delta_s = 0.2\Delta_0$ . In all panels, curves a (solid line), b (dotted line) and c (dashed line) denote  $\varepsilon_b/\Delta_0$ ,  $\Delta_1/\Delta_0$  and  $\Delta_2/\Delta_0$ , respectively.

It is very interesting to clarify how the above novel types of ABS are reflected in the charge transport property [9]. The Hamiltonian  $\hat{H}_N$  in a normal metal is given by putting  $\hat{\Delta}(\mathbf{k}) = 0$  and  $\lambda = 0$  in  $\hat{H}_S$ . We assume an insulating barrier at  $x = 0$  expressed by a delta-function potential  $U\delta(x)$ . The wave function for spin  $\gamma = (\uparrow, \downarrow)$  in

the normal metal  $\Psi_N(x)$  is given by

$$\Psi_N(x) = \exp(ik_F y) \left[ (\psi_{i\gamma} + \sum_{\rho=\uparrow,\downarrow} a_{\gamma,\rho} \psi_{a\rho}) \exp(ik_F x) + \sum_{\rho=\uparrow,\downarrow} b_{\gamma,\rho} \psi_{b\rho} \exp(-ik_F x) \right] \quad (7)$$

with  ${}^T\psi_{i\uparrow} = {}^T\psi_{b\uparrow} = (1, 0, 0, 0)$ ,  ${}^T\psi_{i\downarrow} = {}^T\psi_{b\downarrow} = (0, 1, 0, 0)$ ,  ${}^T\psi_{a\uparrow} = (0, 0, 1, 0)$ , and  ${}^T\psi_{a\downarrow} = (0, 0, 0, 1)$ . The corresponding  $\Psi_S(x)$  is given by Eq. (2). The coefficients  $a_{\gamma,\rho}$  and  $b_{\gamma,\rho}$  are determined by the boundary condition  $\Psi_N(0) = \Psi_S(0)$ , and  $\hbar v_{Sx} \Psi_S(0) - \hbar v_{Nx} \Psi_N(0) = -2iU\tilde{\tau}_3 \Psi_S(0)$  with  $\hbar v_{S(N)x} = \partial \hat{H}_{S(N)} / \partial k_x$ , and diagonal matrix  $\tilde{\tau}_3$  given by  $\tilde{\tau}_3 = \text{diag}(1, 1, -1, -1)$ .

The quantity of interest is the angle averaged charge conductance  $\sigma_C$  given by

$$\sigma_C = \frac{\int_{-\pi/2}^{\pi/2} f_C(\phi) d\phi}{\int_{-\pi/2}^{\pi/2} f_{NC}(\phi) d\phi}, \quad (8)$$

$$f_C(\phi) = [2 + \sum_{\gamma,\rho} (|a_{\gamma,\rho}|^2 - |b_{\gamma,\rho}|^2)] \frac{\cos \phi}{2}, \quad (9)$$

where  $f_{NC}(\phi)$  denotes the angle resolved charge conductance in the normal state with  $\hat{\Delta}(\mathbf{k}) = 0$ . Here,  $\phi$  denotes the injection angle measured from the normal to the interface with  $\sin \phi = k_y/k_f$ . To characterize transparency of the junction interface, we introduce dimensionless constant  $Z = 2mU/\hbar^2 k_f$ .

We plot bias voltage  $eV = E$  dependence of  $\sigma_C$  for  $d_{xy} + p$ -wave case in Fig. 3 for various  $Z$ . First we concentrate on low transparent junction with  $Z = 5$  by changing the value of  $\Delta_s$  and  $\Delta_t$ . At  $\Delta_t = \Delta_s$ , one of the energy gap of the Fermi surface closes corresponding to the quantum phase transition. Then, the resulting  $\sigma_C$  has a gradual change from the quantum critical point. For the case without spin-orbit coupling ( $\beta = 0$ ) with  $\Delta_t > \Delta_s$ ,  $\sigma_C$  has a gap like structure around zero bias due to the absence of Majorana bound state as shown in Figs. 1(A) and 1(B). For  $\Delta_s > \Delta_t$ , ZBCP appears reflecting the zero energy ABS[17]. In the presence of spin-orbit coupling,  $\sigma_C$  always has a ZBCP independent of the ratio of  $\Delta_s$  and  $\Delta_t$  as shown in Fig. 3(B). For  $\Delta_t > \Delta_s$ , the ZBCP originates from purely TRI Majorana bound state. The width of the ZBCP for  $\Delta_t > \Delta_s$  is enhanced with the increase of  $\beta$ , since the region of  $k_y$  where the TRI Majorana bound state exists is expanded with  $\beta$ . For  $\Delta_s > \Delta_t$ , both the conventional ABS and TRI Majorana bound state contribute to the formation of ZBCP. We also plot corresponding  $\sigma_C$  for high ( $Z = 1$ ) and intermediate ( $Z = 2$ ) transparent junctions. For  $\Delta_t > \Delta_s$ ,  $\sigma_C$  has a broad dip-like structure around  $eV = 0$  for  $Z = 1$ , while it is slightly enhanced around  $eV = 0$  for  $Z = 2$  (curves a and b in Figs. 3(C) and (D)). On the other hand, for  $\Delta_s > \Delta_t$ ,  $\sigma_C$  always has a ZBCP (curves d and e in Figs. 3(C) and (D)). The presence of

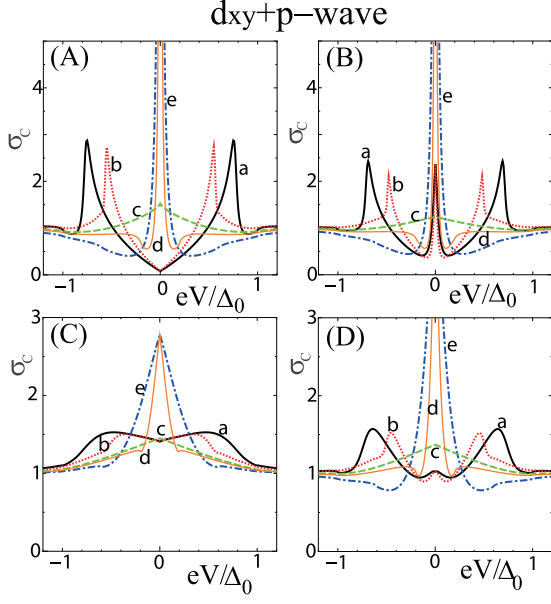


FIG. 3: (Color online) Tunneling conductance  $\sigma_C$  for  $d_{xy} + p$ -wave case. A:  $Z = 5$ ,  $\beta = 0$ , B:  $Z = 5$ ,  $\beta = 0.5$ , C:  $Z = 1$ ,  $\beta = 0.5$ , D:  $Z = 2$ ,  $\beta = 0.5$ . a(solid line):  $\Delta_t = \Delta_0$ ,  $\Delta_s = 0$ , b(dotted line):  $\Delta_t = 0.8\Delta_0$ ,  $\Delta_s = 0.2\Delta_0$ , c(dashed line):  $\Delta_t = 0.5\Delta_0$ ,  $\Delta_s = 0.5\Delta_0$ , d(thin solid line):  $\Delta_t = 0.4\Delta_0$ ,  $\Delta_s = 0.6\Delta_0$ , and e(dot-dashed line):  $\Delta_t = 0.2\Delta_0$ ,  $\Delta_s = 0.8\Delta_0$ .

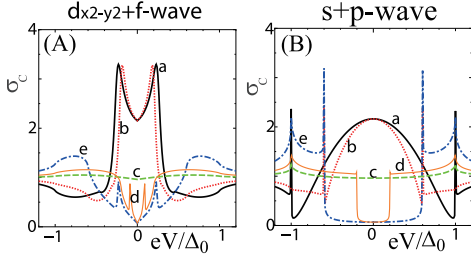


FIG. 4: (Color online) Tunneling conductance  $\sigma_C$  with  $\beta = 0.5$  and  $Z = 5$ . A:  $d_{x^2-y^2} + f$ -wave and B:  $s + p$ -wave. a(solid line):  $\Delta_t = \Delta_0$ ,  $\Delta_s = 0$ , b(dotted line):  $\Delta_t = 0.8\Delta_0$ ,  $\Delta_s = 0.2\Delta_0$ , c(dashed line):  $\Delta_t = 0.5\Delta_0$ ,  $\Delta_s = 0.5\Delta_0$ , d(thin solid line):  $\Delta_t = 0.4\Delta_0$ ,  $\Delta_s = 0.6\Delta_0$ , and e(dot-dashed line):  $\Delta_t = 0.2\Delta_0$ ,  $\Delta_s = 0.8\Delta_0$ .

TRI Majorana bound state gives a clear ZBCP with the increase of  $Z$ . As a reference, the tunneling conductance  $\sigma_C$  for  $d_{x^2-y^2} + f$ -wave and  $s + p$ -wave cases are plotted in Fig. 4 for  $Z = 5$ . ABS exists only for  $\Delta_s < \Delta_t$ . The  $\sigma_C$  for  $d_{x^2-y^2} + f$ -wave has a ZBCP splitting reflecting the complex dispersion  $\varepsilon_b$  shown in Fig. 4(A). On the other hand, for  $s + p$ -wave case,  $\sigma_C$  has a broad ZBCP shown in Fig. 4(B). Summarizing Figs. 3 and 4,  $\sigma_C$  for each pairing state are qualitatively different from each other, which can be used to identify these pairings.

In conclusion, we have studied the ABS and resulting

charge transport for  $d_{xy} + p$ -wave and  $d_{x^2-y^2} + f$ -wave superconductors. We find that the obtained dispersion of ABS in both cases have an anomalous structure. For  $d_{xy} + p$ -wave case, a novel TRI Majorana bound state is generated due to the spin-orbit coupling. The resulting charge conductance can serve as a guide to identify the TRI Majorana bound state and pairing symmetry of NCS superconductors by tunneling spectroscopy.

This work is partly supported by the Sumitomo Foundation (M.S.) and the Grant-in-Aids for Scientific Research No. 22103005 (Y.T. and M.S.), No. 20654030 (Y.T.) and No.22540383 (M.S.).

- 
- [1] E. Bauer, *et. al.*, Phys. Rev. Lett. **92**, 027003 (2004).
  - [2] K. Togano *et al.*, Phys. Rev. Lett. **93**, 247004 (2004); M. Nishiyama, *et al.*, Phys. Rev. B **71**, 220505(R) (2005).
  - [3] P. A. Frigeri, *et. al.*, Phys. Rev. Lett. **92**, 097001 (2004).
  - [4] N. Reyren *et al.*, Science **317**, 1196 (2007).
  - [5] L. P. Gor'kov and E. I. Rashba, Phys. Rev. Lett. **87** 037004 (2001).
  - [6] S. Fujimoto, J. Phys. Soc. Jpn. **76**, 051008 (2007).
  - [7] Y. Yanase and M. Sigrist, J. Phys. Soc. Jpn. **77**, 124711 (2008); Y. Tada, *et al.*, New J. Phys. **11**, 055070 (2009).
  - [8] J. Linder and A. Sudbø, Phys. Rev. B **76**, 054511 (2007).
  - [9] T. Yokoyama, *et al.*, Phys. Rev. B **72** 220504(R) (2005); C. Iniotakis, *et. al.*, Phys. Rev. B **76**, 012501 (2007); M. Eschrig, *et al.*, arXiv:1001.2486.
  - [10] A.B. Vorontsov, *et al.*, Phys. Rev. Lett. **101**, 127003 (2008).
  - [11] Y. Tanaka, *et al.*, Phys. Rev. B **79**, 060505(R) (2009).
  - [12] M. Sato, Phys. Rev. B **73** 214502 (2006); M. Sato and S. Fujimoto, Phys. Rev. B **79**, 094504 (2009).
  - [13] C. K. Lu and S. Yip, Phys. Rev. B **80**, 024504 (2009).
  - [14] T. Yokoyama, *et al.*, Phys. Rev. B **75**, 172511 (2007); T. Yokoyama, *et al.*, J. Phys. Soc. Jpn. **77** 064711 (2008).
  - [15] K. Yada, *et al.*, Phys. Rev. B **80** 140509 (2009).
  - [16] L. J. Buchholtz and G. Zwicknagl, Phys. Rev. B **23**, 5788 (1981); C. R. Hu, Phys. Rev. Lett. **72**, 1526 (1994).
  - [17] Y. Tanaka and S. Kashiwaya, Phys. Rev. Lett. **74**, 3451 (1995); S. Kashiwaya and Y. Tanaka, Rep. Prog. Phys. **63**, 1641 (2000); A. Biswas *et al.*, Phys. Rev. Lett. **88**, 207004 (2002); B. Chesca *et al.*, Phys. Rev. B **71**, 104504 (2005), *ibid.*, **73**, 014529 (2006); **77**, 184510 (2008); M. Wagenknecht *et al.*, Phys. Rev. Lett. **100**, 227001 (2008).
  - [18] F. Wilczek, Nature Phys. **5**, 614 (2009).
  - [19] For example, L. Fu and C. L. Kane, Phys. Rev. Lett. **100**, 096407 (2008); M. Sato, *et al.*, Phys. Rev. Lett. **103**, 020401 (2009); Y. Tanaka, *et. al.*, Phys. Rev. Lett. **103**, 107002 (2009); J. Linder, *et. al.*, Phys. Rev. Lett. **104**, 067001 (2010).
  - [20] When the symmetry of the singlet component of pair potential is  $d_{xy}$ -wave ( $d_{x^2-y^2}$ -wave), the number of the sign change of the real or imaginary part of triplet one on the Fermi surface is two (six). Thus, we call the mixed pair potential  $d_{xy} + p$ -wave ( $d_{x^2-y^2} + f$ -wave).
  - [21] A. P. Schnyder, *et. al.*, Phys. Rev. B **78**, 195125 (2008). X.L. Qi, *et. al.*, Phys. Rev. Lett. **102**, 187001 (2009); R. Roy, arXiv:0803.2881; M. Sato, Phys. Rev. B **79**, 214526 (2009); *ibid.* **81**, 220504(R) (2010).